ARTICLES
PUBLISHED ONLINE: 4 MAY 2014 | DOI: 10.1038/NMAT3950
nature materials

Polariton-mediated energy transfer between organic dyes in a strongly coupled optical microcavity

David M. Coles[1†], Niccolo Somaschi[2,3], Paolo Michetti[4], Caspar Clark[5], Pavlos G. Lagoudakis[2], Pavlos G. Savvidis[6,7] and David G. Lidzey[1*]

Strongly coupled optical microcavities containing different exciton states permit the creation of hybrid-polariton modes that can be described in terms of a linear admixture of cavity-photon and the constituent excitons. Such hybrid states have been predicted to have optical properties that are different from their constituent parts, making them a test bed for the exploration of light–matter coupling. Here, we use strong coupling in an optical microcavity to mix the electronic transitions of two J-aggregated molecular dyes and use both non-resonant photoluminescence emission and photoluminescence excitation spectroscopy to show that hybrid-polariton states act as an efficient and ultrafast energy-transfer pathway between the two exciton states. We argue that this type of structure may act as a model system to study energy-transfer processes in biological light-harvesting complexes.

Cavity polaritons are quasiparticles formed in a microcavity when an optical mode couples to an exciton state such that there is a reversible exchange of energy between the photon and exciton. If the characteristic interaction time is longer than the dephasing time, the system is said to be strongly coupled. Strong coupling has been observed in microcavities containing inorganic quantum well structures[1–3] as well as bulk semiconductors[4,5], organic materials including porphyrins[6,7], J-aggregates[8–10], molecular crystals with strong vibronic replicas[11–13] and polymers[14].

So-called hybrid polaritons are formed when two distinct exciton species simultaneously couple to the same cavity mode and undergo optically driven mixing. Interest in this area was initiated by work[15] predicting that mixing between excitonic states in a strongly coupled microcavity could create hybrid states having entirely new optical properties. The original proposal was for coupling between a series of quantum wells and a crystalline organic layer, with the mixed exciton–polaritons combining the high oscillator strength of the organic Frenkel excitons with the large exciton–exciton interaction typical of inorganic Wannier–Mott excitons, attributes that would be favourable for nonlinear switching applications. Since such pioneering work, experimental realizations have been made in which porphyrin molecules were coupled to a III–V semiconductor quantum well[16] or a perovskite thin film[17], with other work variously demonstrating optically driven coupling between cyanine-dye J-aggregates[18,19] or energetically detuned quantum wells[20]. Recently, optically driven coupling between two molecular dyes has been evidenced in a one-dimensional photonic crystal[21]. Despite such interest, the possibility of using optically driven mixing to facilitate energy transfer between the different states has not yet been demonstrated.

Here, we explore the optical properties of a microcavity containing two strongly coupled J-aggregated cyanine dyes. We show using photoluminescence (PL) emission and PL excitation (PLE) spectroscopy that there is a relaxation pathway created between exciton states mediated by the presence of the mixed exciton–polariton states. We use a rate-equation model describing the population, depopulation and transfer between polariton and exciton states, and show that it provides an excellent description of the measured PL emission. We argue that the observation of energy transfer in the strong coupling regime represents a model system in which to study the coherent dipole–dipole energy-transfer processes that are observed in biological light-harvesting complexes[22,23].

The microcavity structure that we have studied is shown schematically in Fig. 1 and consisted of two silver mirrors between which was deposited a thin-film blend of the cyanine dyes 5,6-dichloro-2-[[5,6-dichloro-1-ethyl-3-(4-sulphobutyl)-benzimidazol-2-ylidene]-propenyl]-1-ethyl-3- (4-sulphobutyl)-benzimidazolium hydroxide, sodium salt, inner salt (TDBC, FEW Chemicals) and 5-chloro-2-[3-[5-chloro-3-(3-sulphopropyl-2(3H)-benzothiazolylidene]-2-methyl-1-propenyl]-3-(3-sulphopropyl) benzothiazolium hydroxide, inner salt, compound with triethylamine (NK-2707, Hayashibara Biochemical). The dyes TDBC and NK-2707 both undergo self-organization in a suitable solvent to form J-aggregates whose absorption and emission are characterized by an intense and narrow J-band as shown in the insets to Fig. 2a. Such characteristics have made J-aggregates an ideal system to study strong coupling in optical microcavities[24].

[1]Department of Physics and Astronomy, University of Sheffield, Hicks Building, Hounsfield Road, Sheffield S3 7RH, UK, [2]School of Physics and Astronomy, University of Southampton, Southampton SO17 1BJ, UK, [3]IESL-FORTH, PO Box 1527, 71110 Heraklion, Crete, Greece, [4]Institute of Theoretical Physics, Technische Universität Dresden, 01062 Dresden, Germany, [5]Helia Photonics, Rosebank Park, Livingston EH54 7EJ, UK, [6]IESL-FORTH, PO Box 1527, 71110 Heraklion, Crete, Greece, [7]Department of Materials Science and Technology, University of Crete, 71003 Heraklion, Crete, Greece. †Present address: Department of Materials, University of Oxford, Parks Road, Oxford OX1 3PH, UK. *e-mail: d.g.lidzey@sheffield.ac.uk

Figure 1 | Microcavity structure supporting hybrid organic polaritons. The microcavity structure studied comprised of a 620-nm-thick layer of a blend of two different J-aggregates in a supporting matrix between two metallic mirrors. The cavity was constructed from a 200-nm-thick silver mirror that was thermally evaporated onto a 1-mm-thick quartz substrate. A solution of the TDBC and NK-2707 dyes in an aqueous gelatine solution (5 mg ml^{-1}) mixed at a 3:1 (TDBC/NK-2707) volume ratio was then spin-cast onto the silver mirror to form a film having a thickness of 620 nm. A 35 nm semi-transparent silver mirror was then evaporated directly onto the organic film to complete the cavity. The resultant cavity supported a confined $3\lambda/2$ mode that was positioned approximately 100 meV below that of the lower-lying NK-2707 exciton level. The *Q*-factor of the cavity was approximately 90 (cavity lifetime of $\sim$ 35 fs).

We first present PL and PLE measurements performed on control films consisting of TDBC and NK-2707 J-aggregates dispersed individually into a gelatine matrix and also as a thin-film blend as shown in Fig. 2a. It can be seen that the J-aggregate blend is characterized by two absorption and fluorescence peaks that correspond to the separate absorption and emission transitions of the TDBC and NK-2707 components. As the PL quantum yield and extinction coefficients of the two dyes are different, the mixing ratio between dyes was adjusted such that the PL intensities of both emission peaks were approximately equal. This is to ensure that the radiative pumping of polariton states (discussed in the Methods) is approximately equal for each exciton species. As a result of this, the TDBC absorption peak (at 587.3 nm) is more than 6 times larger than that of the NK-2707 (at 636.4 nm).

A PLE spectrum of a control J-aggregate blend film is shown in Fig. 2b. Here, data were recorded by scanning the excitation laser wavelength and recording PL emission at 636.4 nm (the peak of the NK-2707 J-aggregate emission). The PLE spectrum is characterized by a dip in intensity at a wavelength corresponding to the peak absorption peak of TDBC reflecting the negligible direct energy transfer by dipole–dipole coupling in the control thin film. This conclusion is further supported by the PL emission fluorescence lifetime measurements of a mixed film of TDBC and NK-2707, and a film of TDBC alone in gelatine (dispersed at the same concentration as in the mixed film) as shown in Supplementary Section 1. The PL spectra of both J-aggregates show a biexponential decay, with the initial fast decay component attributed to the exciton–exciton annihilation process[25–29] and the slower component to super-radiant decay of the coupled dipoles within each individual aggregate. Critically however, there are only small changes in the TDBC PL decay lifetime when it is mixed with the NK-2707, indicating that the blend does not act as an efficient donor–acceptor system. We speculate that the limited direct energy transfer between the two exciton species has two origins. First, we calculate a relatively small Förster transfer radius of approximately 0.8 nm (assuming random dipole orientation and using a measured TDBC fluorescence quantum yield of 1.1%) that results from the narrow absorption and emission linewidths and small Stokes Shift of both components. Second, we believe that phase separation in the blend film creates almost pure aggregates of TDBC and NK-2707 that are dispersed within an insulating gelatine matrix, with the length scales of phase separation being sufficiently large to prevent direct dipole–dipole interaction. Atomic force micrographs of the blend surface are presented in Supplementary Section 2; although the film is clearly nanostructured, it is not possible to clearly resolve individual J-aggregate domains.

We now discuss the optical properties of the microcavity system in Fig. 1. The angle-dependent PL emission following non-resonant excitation at 473 nm is shown in Fig. 3. Polariton energies are described by the coupled oscillator model expressed by equation (1), which we use to fit to the polariton PL dispersion, shown as white dotted lines in Fig. 3a.

$$\begin{pmatrix} E_\gamma(\theta) & \hbar\Omega_1/2 & \hbar\Omega_2/2 \\ \hbar\Omega_1/2 & E_{ex1} & 0 \\ \hbar\Omega_2/2 & 0 & E_{ex2} \end{pmatrix} \begin{pmatrix} \alpha_\gamma \\ \alpha_{ex1} \\ \alpha_{ex2} \end{pmatrix} = E_{pol}(\theta) \begin{pmatrix} \alpha_\gamma \\ \alpha_{ex1} \\ \alpha_{ex2} \end{pmatrix} \quad (1)$$

where $E_\gamma(\theta) = E_0\left(1-\sin^2(\theta)/n^2\right)^{-1/2}$ is the cavity mode energy, E_0 is the cavity cutoff energy and n is the intracavity effective refractive index. E_{ex1} and E_{ex2} are the energies of the two exciton species and $E_{pol}(\theta)$ is the polariton energy. $\hbar\Omega_1$ and $\hbar\Omega_2$ are the light–matter coupling energies. The mixing coefficients $|\alpha_\gamma|^2$, $|\alpha_{ex1}|^2$ and $|\alpha_{ex2}|^2$ describe the relative photonic and excitonic weightings of the polaritons. There are three unique solutions for $E_{pol}(\theta)$ and thus the polariton energy dispersion comprises 3 angle-dependent branches, here termed the upper (UPB), middle (MPB) and lower (LPB) polariton branches.

Polariton branches undergo anti-crossing at points where the photon mode and exciton ex1 or ex2 would have been degenerate, with Rabi splitting energies of $\hbar\Omega_1$ and $\hbar\Omega_2$, respectively. At normal incidence the photon energy is 101 meV below the NK-2707 exciton (for simplicity now referred to as ex1) and 250 meV below the TDBC exciton (referred to as ex2). A Rabi splitting energy of $\hbar\Omega_1 = 73$ meV is determined between the LPB and MPB, whereas there is a larger splitting of $\hbar\Omega_2 = 155$ meV between the MPB and UPB, consistent with the higher oscillator strength ($\mathcal{F}$) contributed from the TDBC J-aggregates (with $\hbar\Omega \propto \sqrt{\mathcal{F}}$; refs 30–32). In Fig. 3c–e, we plot the relative mixing fraction between the cavity photon and the ex1 and ex2 exciton in the UPB, MPB and LPB respectively. It can be seen that there is a clear mixing between the ex1 and ex2 states along the MPB, with maximum mixing occurring at an angle of approximately 38°.

We can relate peak emission intensity (I_{pol}) to the relative polariton population (P_{pol}) at any viewing angle using equation (2).

$$P_{pol} \propto \frac{I_{pol}}{|\alpha_\gamma|^2} \quad (2)$$

We plot the relative population of the polariton branches in Fig. 3b. We find that the LPB population increases as it approaches the energy of the ex1 exciton state. This effect is well understood[32,34–44] and results from polariton states close to the exciton energy, being more effectively populated from the reservoir of uncoupled exciton states by both scattering with vibrations and radiative pumping mechanisms (a process described in more detail in the Methods)[44,45]. The population of polaritons in the LPB is significantly greater than that in either the UPB or MPB at all angles. This observation provides qualitative evidence for an efficient energy relaxation pathway that depopulates both the UPB and MPB. We discount the direct emission of photons by ex2 and subsequent re-absorption by ex1 (photon recycling) as being an important energy-transfer mechanism as if such a process were important, it should be evident from PLE measurements on the control non-cavity film, where instead it is not seen. This is

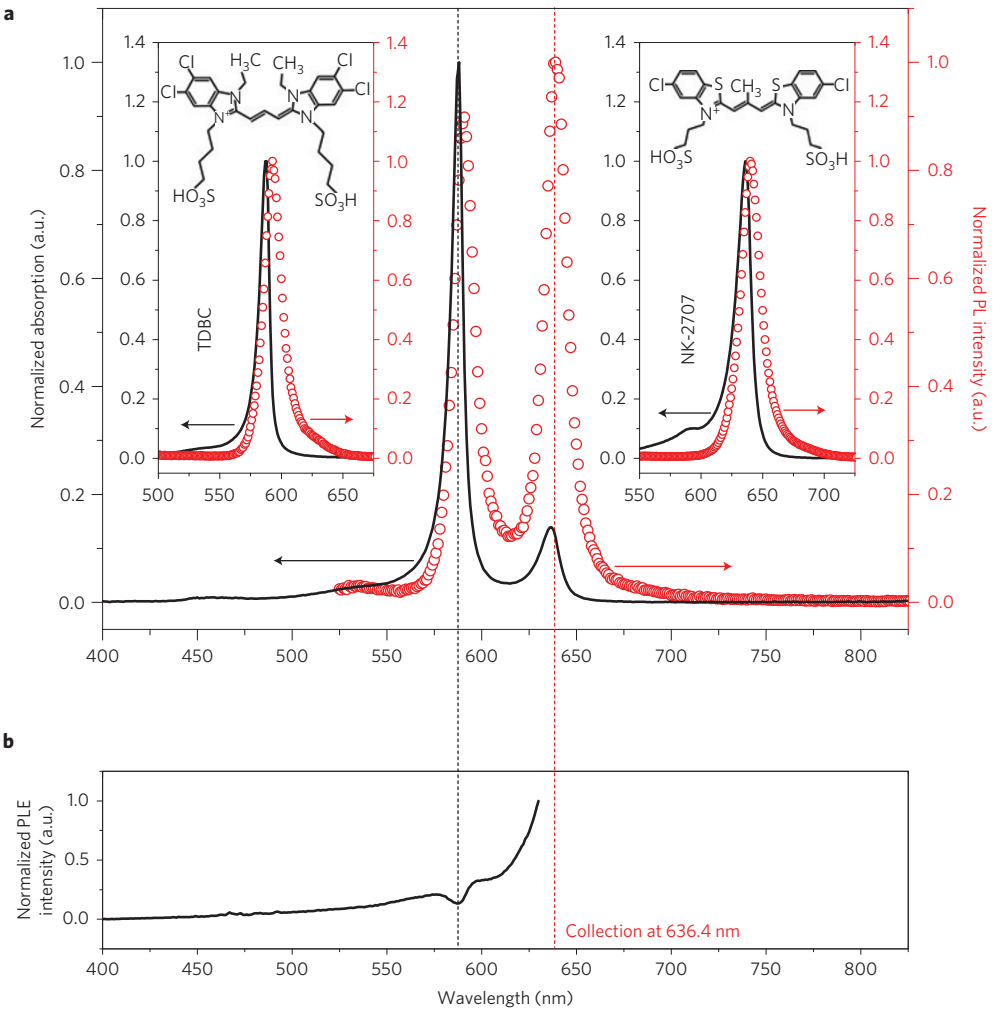

Figure 2 | Characterization of the individual J-aggregates and a blended film. a, Normalized absorption and PL spectra of a mixture of TDBC and NK-2707 in a gelatine matrix (volume ratio 3:1) with the absorption and PL of TDBC and NK-2707 in gelatine shown in the left and right insets, respectively. PL is collected following excitation at 473 nm. **b**, PLE spectrum with detection at the PL peak of NK-2707 (636.4 nm). The black and red dashed lines show the position of the TDBC absorption maximum and NK-2707 photoluminescence maximum, respectively.

due to the limited overlap between the TDBC PL emission and NK-2707 absorption.

We can study the efficiency of relaxation processes using PLE spectroscopy. Figure 4a shows a two-dimensional map of the PLE signal recorded detecting emission from the bottom of the LPB (692 nm at $\theta = 0°$) while scanning the excitation wavelength and angle. In Fig. 4d, we re-plot this data showing the peak PLE signal intensity for each of the polariton branches as a function of external excitation angle. To correct such data for the amount of light absorbed by the cavity at each angle and wavelength, we plot the angle-dependent absorption measured simultaneously with the PLE (see ref. 33 for details). This is shown in Fig. 4b with the magnitude of the absorption for each polariton branch plotted in Fig. 4e. However, the measured absorption includes light absorbed both within the active layer and in the metallic mirrors. We therefore use a transfer matrix approach to calculate the fraction of light absorbed by the mirrors and then correct the measured absorption to determine the absorption of the active layer (discussed in Supplementary Section 3). We find that as expected, the relative absorption of each of the polariton branches approximately follows their photonic fraction (Fig. 3c–e, black lines). We can use these data to obtain the relative efficiency by which each polariton state relaxes to the bottom of the LPB. Figure 4c shows the PLE intensity signal recorded at each angle and wavelength divided by the active-layer absorption. Again, we show the magnitude of this relaxation efficiency for each polariton branch in Fig. 4f.

It can be seen that relaxation efficiency of states along the LPB towards $k_{\parallel} = 0$ is characterized by a broad peak that is centred around 43°. We have previously argued[33] that this results from a polariton bottleneck effect similar to that seen in strongly coupled inorganic-semiconductor microcavities[46,47]. In contrast, the UPB has an approximately uniform relaxation efficiency as a function of angle. A similar observation has been made in PLE measurements performed on cavities containing a single species of J-aggregated dye[33], and was attributed to the fast relaxation of UPB polaritons to the exciton reservoir[48] that was followed by exciton scattering to lower-branch polariton states. In this hybrid cavity, we assume once an UPB polariton returns to the ex2 reservoir, it is then free to scatter into MPB states or otherwise remain in the ex2 reservoir. As we argue below, the MPB presents a channel that facilitates relaxation from the ex2 to the ex1 reservoir from where they can then populate states along the LPB.

Figure 4f indicates that the relaxation efficiency of MPB polaritons to the bottom of the LPB is larger than that observed in either the UPB or from LPB states. We propose that this relaxation process occurs through the decay of MPB states to the ex1 reservoir followed by scattering of ex1 excitons to states at the bottom of the LPB. Clearly the relaxation efficiency of MPB polaritons is

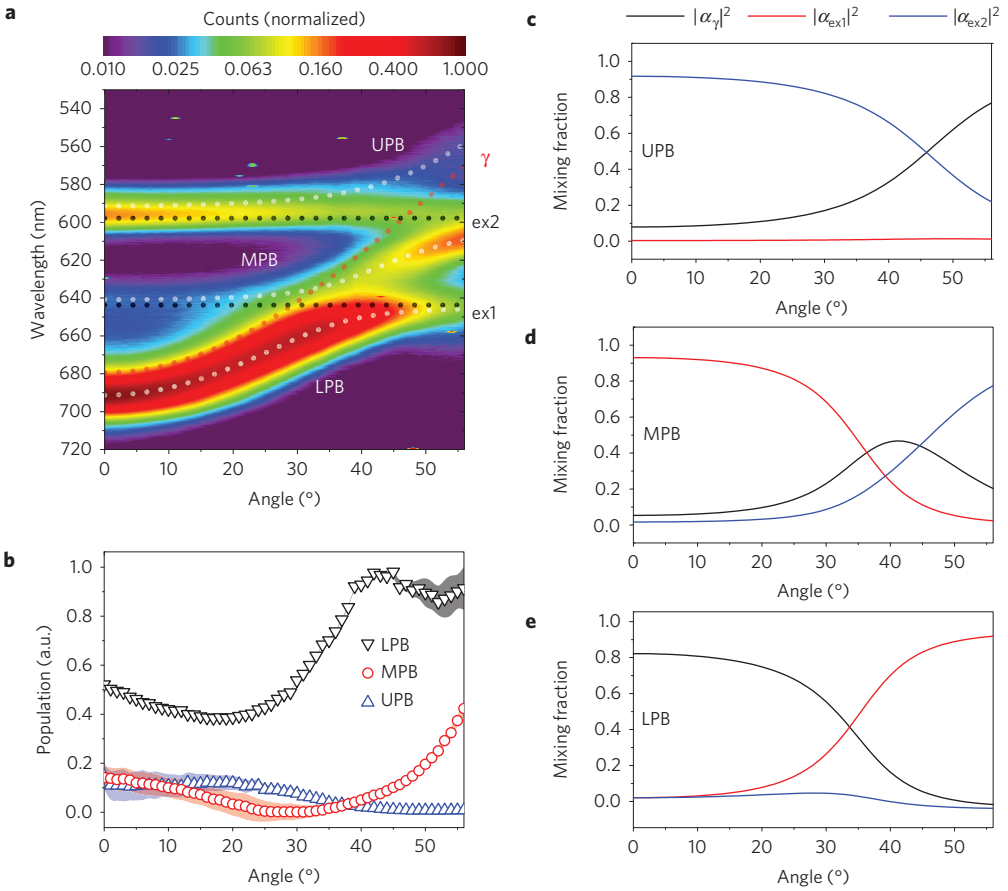

Figure 3 | Hybrid-polariton emission, population and mixing coefficients. a, Angle-dependent microcavity emission following excitation at 473 nm. White dotted lines indicate the position of the polariton branches, and exciton and photon energies are shown with black and red dotted lines respectively, with all features determined using a fit to the PL spectra using equation (1). The colour palette is on a log scale. **b**, Polariton population distributions. The shaded regions represent the experimental uncertainty. **c**–**e**, Polariton branch mixing for the UPB (**c**) MPB (**d**) and LPB (**e**). PL characterization of the cavity was performed at room temperature following the method described in ref. 33.

not constant as a function of angle, a result that suggests that the relative mixing fraction of the two exciton states plays some role in determining the rate of this process. Indeed, it can be seen that the MPB relaxation efficiency increases as its ex1 fraction increases (compare Fig. 4f with Fig. 3d), suggesting a mechanism in which the ex1 component of the MPB states facilitates relaxation by interaction with the local vibrational environment. Interestingly however, it seems that even when the fraction of ex1 exciton mixed into the MPB is very small (order of 2.5%), relaxation to the ex1 reservoir and the LPB is still possible.

Note, we have also performed the same PL/PLE experiments and analysis on control films and strongly coupled cavities in which the two different J-aggregate layers are separated by a 200-nm-thick transparent spacer layer (Supplementary Section 4). Here we observe very similar PL/PLE as observed from the mixed J-aggregate system, confirming that direct dipole–dipole coupling cannot be used to explain our results.

We have used a rate-equation model to describe the population and depopulation of polariton states in the 3 branches to simulate the angle-dependent PL emission. Full details of the model are given in the Methods; however as input to the model, we use the relaxation efficiency plotted in Fig. 4f and the measured PL spectra of the blended J-aggregates (Fig. 2), together with the fitted values for exciton and photon fraction determined using equation (1). A key feature of the model is the ability of excitons to relax to and from states in the MPB, with such states effectively acting as a pathway between the exciton reservoirs. Indeed, our model indicates that states in the MPB are mainly populated through direct scattering from the ex2 reservoir and then are depopulated by both radiative emission and relaxation to the lower-lying ex1 reservoir, with the relaxation time of polaritons to ex1 predicted to be of the order of 10 fs. Using this model, we plot the PL emission intensity for each polariton branch as a function of angle in Fig. 5, together with the best fit to emission intensity.

The good fit between the simple phenomenological model we have described and the PL measurements allows us to derive the following picture describing the relaxation dynamics in this hybrid-polariton system. The UPB is populated by both radiative pumping and thermal promotion of excitons from the ex2 reservoir. The relaxation of UPB polaritons to the ex2 reservoir is much faster than its radiative emission rate. Indeed, the model suggests that the radiative decay channel is responsible for depopulating only 20% of the polaritons in this branch. The MPB is almost entirely populated by the scattering from the higher energy ex2 reservoir whereas it is depopulated through two competing processes: non-radiative relaxation into the ex1 reservoir and direct radiative emission. We find that non-radiative relaxation accounts for the depopulation of over 90% of the polaritons in this branch, explaining the strong suppression of luminescence from most of the MPB. Our results indicate therefore that once an ex2 exciton scatters to an MPB state, it is highly likely to relax to the ex1 reservoir and hence the MPB has the crucial function of exchanging population between the two exciton species. Finally, the LPB is populated by both scattering and radiative pumping from the ex1 reservoir.

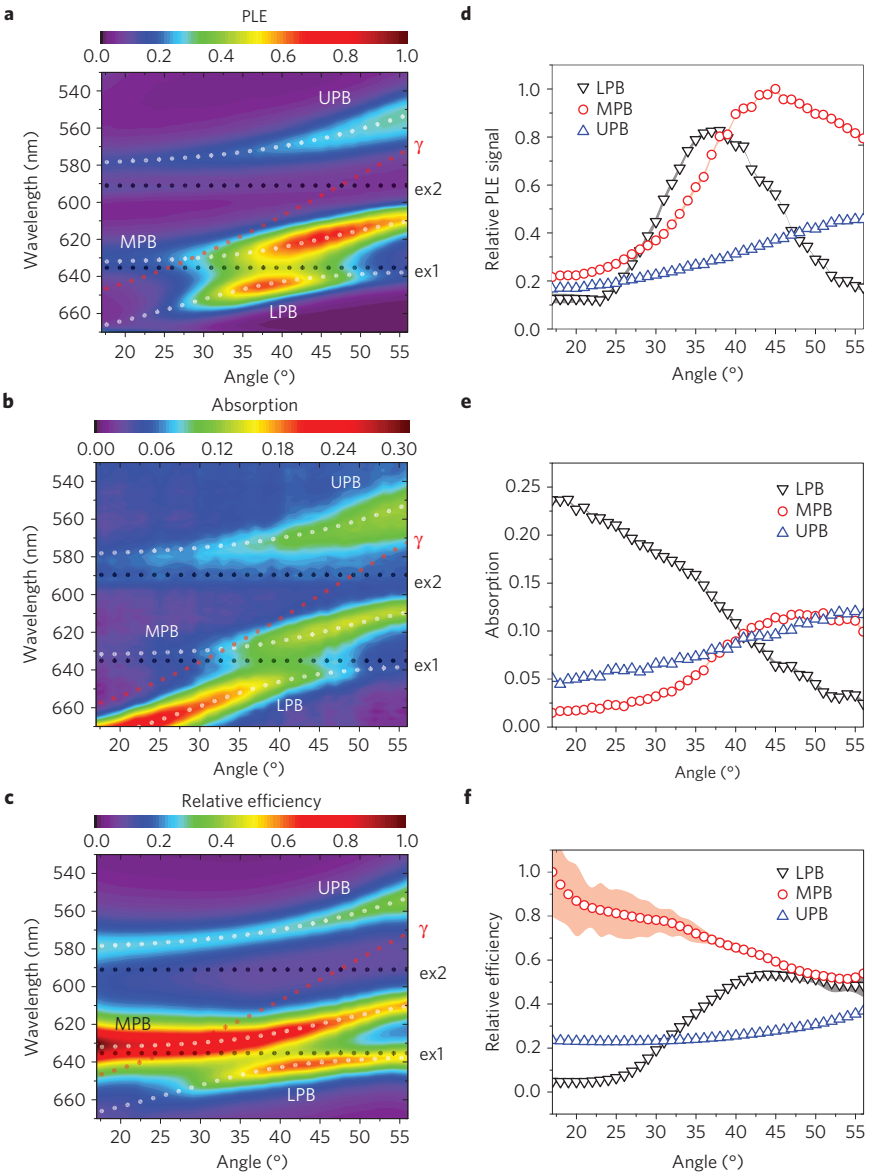

Figure 4 | Angle- and wavelength-dependent PLE of the $k_{\|} = 0$ LPB state, polariton absorption and relative relaxation efficiency into the LPB ground state. a, Angle-dependent PLE signal recorded at $k_{\|} = 0$ on the LPB. **b**, Angle-dependent absorption measured simultaneously with PLE. **c**, Angle-dependent relative relaxation efficiency to $k_{\|} = 0$ on the LPB. The white, red and black dotted lines show the same as in Fig. 3a. **d**–**f**, The magnitude of the PLE (**d**), absorption (**e**) and efficiency (**f**) for each branch. The shaded regions represent the experimental uncertainty. PLE characterization of the cavity was performed at room temperature following the method described in ref. 33.

To confirm this picture, we have also studied cavities in which the cavity photon at normal incidence is positioned at a higher energy than that of the ex1 and ex2 excitons, allowing us to reduce the relative degree of mixing between the cavity-photon and the exciton states in the MPB. Qualitatively, we find that as mixing is reduced, the relative population of the MPB increases (with respect to the LPB), consistent with a reduced efficiency of energy transfer (Supplementary Section 5).

The ultrafast decay dynamics predicted by our model indicate that a number of processes are likely to contribute to the relaxation of MPB polaritons. These include interactions with both vibrational modes of the cyanine dye molecules and a degenerate tail of ex1 states together with other dephasing mechanisms. Despite such fast MPB polariton decay processes our PL decay dynamics measurements (presented in Supplementary Section 6) indicate that the overall decay dynamics of the exciton reservoirs are not significantly modified as a result of strong coupling. Such results can be reconciled with the fact that the exciton to polariton scattering rate is relatively slow (order of 300 ps; ref. 44) and thus this is a relatively inefficient exciton decay channel, with disorder limiting the relative fraction of polariton states to between 0.3 and 4×10^{-4} depending on Rabi-splitting energy and exciton–photon detuning[32,45]. We note that only excitons that have scattered into the MPB are involved in the exciton–exciton transfer process, and hence this fraction puts an upper bound on the fraction of ex2 reservoir excitons that transfer to the ex1 reservoir.

We have studied the decay dynamics of hybrid organic polaritons and find that a relaxation pathway is formed between two exciton species that is dependent on the exciton mixing present in the MPB. Such a process represents a new non-radiative energy-transfer mechanism that can transfer populations between exciton states that are separated by length scales much greater than the Förster transfer radius. Indeed, we have recently evidenced strong coupling in a microcavity in which the organic film had

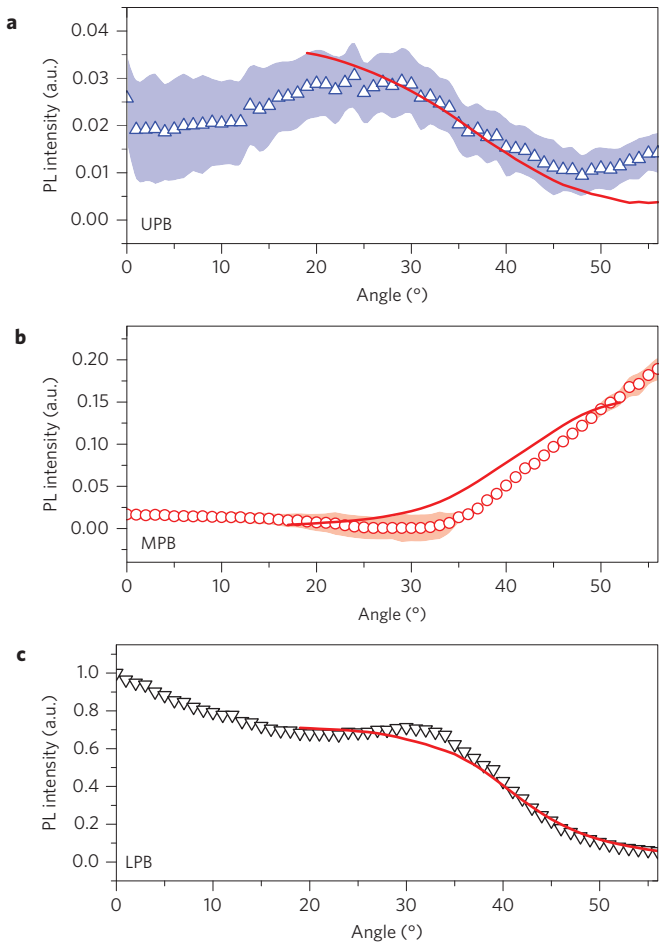

Figure 5 | Modelling of the polariton emission. a–c, Observed polariton emission intensity (open symbols) following non-resonant continuous-wave excitation at 473 nm, and modelled intensity (solid lines) for the UPB (**a**), MPB (**b**) and LPB (**c**). The shaded regions represent the experimental uncertainty.

a thickness of several micrometres, a length scale that provides an upper bound for the energy-transfer process demonstrated here. We believe that the processes explored here serve as an interesting model to study energy transfer in light-harvesting complexes. Two-dimensional spectroscopy results demonstrate that coherent coupling between chromophores mediated by resonant dipole–dipole coupling permits energy transfer to occur over surprisingly large distances at room temperature[22,23]. There are distinct similarities with the results shown here, where we have shown the transfer of energy between states coupled by a real photon similarly drives energy transfer over mesoscopic distances (of the order of the length of the cavity) and that this process is expected to be fast and efficient. The role of polariton coherence in this energy-transfer process is not yet understood; however, unravelling such ultrafast dynamics in the model structures explored here is likely to have relevance in a range of both natural and synthetic light-harvesting systems.

Methods

We have developed a simple model based on a series of rate equations to better understand the effectiveness of the different relaxation pathways in our system and hence explain the angle-dependent PL emission of the UPB, MPB and LPB. Following the non-resonant pumping of the system, a rapid thermalization of molecular excitations creates a build-up and then steady-state population of the ex1 and ex2 species in the exciton reservoirs[34] that can (for all practical purposes) be considered constant. Therefore, we account only for the processes that

Table 1 | Fitting parameters used in equations (3)–(5) to produce Fig. 5 in the main text.

$C_1 = (228\ \text{ps})^{-1}$	$C_5^{LPB} = (295\ \text{fs})^{-1}$	$p_1 = 1.93$
$C_2 = (603\ \text{ps})^{-1}$	$C_5^{MPB} = (8.5\ \text{fs})^{-1}$	$p_2 = 0$
$C_3 = (36\ \text{ps})^{-1}$	$C_5^{UPB} = (34\ \text{fs})^{-1}$	
$C_4 = (35\ \text{fs})^{-1}$		

The constants are scaled such that C_4 is equal to $(35\ \text{fs})^{-1}$ and hence the polariton radiative decay rate equals the cavity-photon decay rate when the photonic component is equal to unity. We note that the ratios between C_1, C_2 and C_3 are fixed, as is the ratio C_4 to C_5. It is these ratios that define the shape of the fit. As we measure only the relative number of polaritons, we normalize the data such that the ratio of the scattering rates $C_1/C_4 \sim 10^{-4}$, an assumption based on previous theoretical work[34,38,39]. Note that the term that describes the optical pumping of the three polariton branches is described by the product of the constant C_3 multiplied by the PL overlap factor P_X. As this PL overlap factor is arbitrarily normalized to unity, we cannot directly compare the magnitude of rate constants C_1 and C_2 with C_3. The fast decay lifetime of the MPB (~10 fs) is in good agreement with its experimentally determined linewidth (~58 meV or 5.7 fs); however, we believe the linewidth of the polariton branches is also broadened by both photonic and excitonic disorder, a feature that explains their weak linewidth dependence on measurement angle.

populate and deplete states along the polariton branches. Equations (3), (4) and (5) describe the time-dependent change in the (angle-dependent) mean polariton population (N) in states bound by the observation angle in the LPB, MPB and UPB respectively. These equations are not directly coupled as direct inter-branch relaxation is prevented as it is very much slower (in the linear regime) than polariton radiative decay or non-radiative relaxation to exciton-reservoir states at lower energy[34–36]. The equations instead describe the population exchange between the polariton branches and the two exciton reservoirs. We solve for the steady-state condition ($dN/dt = 0$), and fit the predicted polariton photoluminescence emission to the experimental data as shown in Fig. 5.

$$\frac{dN_{LPB}}{dt} = C_1|\alpha_{ex1}^{LPB}|^2(B_1+1)\left(\frac{\Delta E_1}{J}\right)^{p_1} + C_3 P_{LPB}|\alpha_\gamma^{LPB}|^2 - N_{LPB}C_4|\alpha_\gamma^{LPB}|^2 - N_{LPB}C_5^{LPB}R_{LPB} = 0 \quad (3)$$

$$\frac{dN_{MPB}}{dt} = C_2|\alpha_{ex2}^{MPB}|^2(B_2+1)\left(\frac{\Delta E_2}{J}\right)^{p_2} + C_1|\alpha_{ex1}^{MPB}|^2 B_1\left(\frac{\Delta E_1}{J}\right)^{p_1} + C_3 P_{MPB}|\alpha_\gamma^{MPB}|^2 - N_{MPB}C_4|\alpha_\gamma^{MPB}|^2 - N_{MPB}C_5^{MPB}R_{MPB} = 0 \quad (4)$$

$$\frac{dN_{UPB}}{dt} = C_2|\alpha_{ex2}^{UPB}|^2 B_2\left(\frac{\Delta E_2}{J}\right)^{p_2} + C_3 P_{UPB}|\alpha_\gamma^{UPB}|^2 - N_{UPB}C_4|\alpha_\gamma^{UPB}|^2 - N_{UPB}C_5^{UPB}R_{UPB} = 0 \quad (5)$$

These equations also include the following terms:

$$B_\sigma = \left(\exp\left[\frac{\Delta E_\sigma}{kT}\right] - 1\right)^{-1}, \quad \Delta E_\sigma = |E_{pol} - E_{ex\sigma}|$$

with $\sigma = 1$ or 2.

The equations include terms that describe the scattering from exciton reservoir exσ to a polariton branch, mediated by the absorption ($\propto B_\sigma$) or emission ($\propto 1 + B_\sigma$) of a molecular vibration, where the thermal bath of molecular vibrations is populated according the Bose–Einstein distribution. These terms are proportional to the parameters C_1 and C_2 when describing exciton reservoirs ex1 and ex2 respectively, and scale with the excitonic component $|\alpha_{ex\sigma}|^2$ of the polariton (as scattering preferentially occurs into exciton-like states). These terms scale with the polariton–exciton energy separation $|\Delta E_\sigma|$, with scattering being more rapid for larger energetic separations. This process is introduced in a phenomenological way[34], so that the terms are proportional to $(\Delta E_\sigma/J)^{p_\sigma}$, where $J = 75$ meV, with p_σ left as a fitting parameter[34]. The LPB (UPB) mainly contains ex1 (ex2)-like states; therefore, equation (3) (equation (5)) accounts only for the scattering from the ex1 (ex2) reservoir. The MPB has an intrinsic hybrid nature and can therefore exchange particles with both ex1 and ex2 exciton reservoirs, creating a relaxation pathway between the two exciton species.

The terms proportional to the parameter C_3 describe the direct radiative pumping of polariton states through radiative decay of weak-coupled excitons in

the exciton reservoir, with the emitted photon being absorbed by the photonic component of a polariton state[44]. We describe this term as the product of the photon fraction mixed into the polariton branch ($|\alpha_\gamma^X|^2$), where X = LPB, MPB or UPB, with the relative PL intensity [$P_X(\theta)$] from the reservoirs (determined from a non-cavity control film) at each particular polariton energy. We normalize the total PL overlap such that $\sum_X^{\mathrm{LPB,MPB,UPB}} \int_{17°}^{56°} P_X(\theta)d\theta = 1$. The term described by constant C_4 represents the radiative decay of polaritons, and is proportional to the photonic component of each state.

The final term (including fitting constant C_5) describes non-radiative relaxation of polaritons to the exciton reservoir[34,35,48]. We describe the relative efficiency of the relaxation process [$R_X(\theta)$] using the measured PLE relaxation efficiency data for each polariton branch as a function of angle as plotted in Fig. 4f. We normalize R_X to 1 for each branch (to high angle on the LPB, or 0° on the UPB and MPB). This allows us to make an order-of-magnitude estimate of the scattering rate to the exciton reservoirs. The measured PLE relaxation efficiency data describe the efficiency by which any polariton state relaxes to the bottom of the LPB (passing through the exciton reservoirs), and its use here to describe the overall probability that any polariton state along the LPB undergoes any form of energetic relaxation is clearly an approximation. Note we can also describe this relaxation process on the basis of the exciton fraction of the initial and final states involved as shown in Supplementary Section 7, and obtain a similar fit to the cavity emission data.

We solve these equations to determine N for each branch as a function of angle. The photoluminescence intensity from the cavity can then be calculated as a function of angle using equation (2). We summarize the parameters used in our model in Table 1. We note that the fitting value of p_2 is zero, which is mainly due to the relative small energy separation between the exciton reservoir ex2 and the polariton states of UPB and MPB, which does not allow us to accurately determine this parameter. For the LPB, the relatively large energetic separation from the ex1 exciton reservoir allows us to determine a finite value for p_1.

Received 19 November 2013; accepted 18 March 2014; published online 4 May 2014

References

1. Weisbuch, C., Nishioka, M., Ishikawa, A. & Arakawa, Y. Observation of the coupled exciton–photon mode splitting in a semiconductor quantum microcavity. *Phys. Rev. Lett.* **69,** 3314–3317 (1992).
2. Houdré, R. *et al.* Measurement of cavity-polariton dispersion curve from angle-resolved photoluminescence experiments. *Phys. Rev. Lett.* **73,** 2043–2046 (1994).
3. Tassone, F., Piermarocchi, C., Savona, V., Quattropani, A. & Schwendimann, P. Bottleneck effects in the relaxation and photoluminescence of microcavity polaritons. *Phys. Rev. B* **56,** 7554–7563 (1997).
4. Butté, R. *et al.* Room-temperature polariton luminescence from a bulk GaN microcavity. *Phys. Rev. B* **73,** 033315 (2006).
5. Christopoulos, S. *et al.* Room-temperature polariton lasing in semiconductor microcavities. *Phys. Rev. Lett.* **98,** 126405 (2007).
6. Lidzey, D. G. *et al.* Strong exciton–photon coupling in an organic semiconductor microcavity. *Nature* **395,** 53–55 (1998).
7. Savvidis, P. G., Connolly, L. G., Skolnick, M. S., Lidzey, D. G. & Baumberg, J. J. Ultrafast polariton dynamics in strongly coupled zinc porphyrin microcavities at room temperature. *Phys. Rev. B* **74,** 113312 (2006).
8. Lidzey, D. G. *et al.* Room temperature polariton emission from strongly coupled organic semiconductor microcavities. *Phys. Rev. Lett.* **82,** 3316–3319 (1999).
9. Schouwink, P., Berlepsch, H. V., Dähne, L. & Mahrt, R. F. Observation of strong exciton–photon coupling in an organic microcavity. *Chem. Phys. Lett.* **344,** 352–356 (2001).
10. Tischler, J. R., Bradley, M. S., Bulović, V., Song, J. H. & Nurmikko, A. Strong coupling in a microcavity LED. *Phys. Rev. Lett.* **95,** 036401 (2005).
11. Holmes, R. J. & Forrest, S. R. Strong exciton–photon coupling and exciton hybridization in a thermally evaporated polycrystalline film of an organic small molecule. *Phys. Rev. Lett.* **93,** 186404 (2004).
12. Kéna-Cohen, S., Davanço, M. & Forrest, S. R. Strong exciton–photon coupling in an organic single crystal microcavity. *Phys. Rev. Lett.* **101,** 116401 (2008).
13. Kéna-Cohen, S. & Forrest, S. Room-temperature polariton lasing in an organic single-crystal microcavity. *Nature Photon.* **4,** 371–375 (2010).
14. Takada, N., Kamata, T. & Bradley, D. D. C. Polariton emission from polysilane-based organic microcavities. *Appl. Phys. Lett.* **82,** 1812–1814 (2003).
15. Agranovich, V., Benisty, H. & Weisbuch, C. Organic and inorganic quantum wells in a microcavity: Frenkel–Wannier–Mott excitons hybridization and energy transformation. *Solid State Commun.* **102,** 631–636 (1997).
16. Holmes, R. J., Kéna-Cohen, S., Menon, V. M. & Forrest, S. R. Strong coupling and hybridization of Frenkel and Wannier–Mott excitons in an organic–inorganic optical microcavity. *Phys. Rev. B* **74,** 235211 (2006).
17. Wenus, J. *et al.* Hybrid organic–inorganic exciton–polaritons in a strongly coupled microcavity. *Phys. Rev. B* **74,** 235212 (2006).
18. Lidzey, D. G., Bradley, D. D. C., Armitage, A., Walker, S. & Skolnick, M. S. Photon-mediated hybridization of Frenkel excitons in organic semiconductor microcavities. *Science* **288,** 1620–1623 (2000).
19. Lidzey, D. G. *et al.* Hybrid polaritons in strongly coupled microcavities: experiments and models. *J. Lumin.* **110,** 347–353 (2004).
20. Wainstain, J. *et al.* Dynamics of polaritons in a semiconductor multiple-quantum-well microcavity. *Phys. Rev. B* **58,** 7269–7278 (1998).
21. Lodden, G. H. & Holmes, R. J. Long-range, photon-mediated exciton hybridization in an all-organic, one-dimensional photonic crystal. *Phys. Rev. Lett.* **109,** 096401 (2012).
22. Engel, G. S. *et al.* Evidence for wavelike energy transfer through quantum coherence in photosynthetic systems. *Nature* **446,** 782–786 (2007).
23. Collini, E. *et al.* Coherently wired light-harvesting in photosynthetic marine algae at ambient temperature. *Nature* **463,** 644–647 (2010).
24. Tischler, J. R. *et al.* Solid state cavity QED: Strong coupling in organic thin films. *Org. Electron.* **8,** 94–113 (2007).
25. Brumbaugh, D. V., Muenter, A. A., Knox, W., Mourou, G. & Wittmershaus, B. Singlet exciton annihilation in the picosecond fluorescence decay of 1,1'-diethyl-2,2'-cyanine chloride dye j-aggregate. *J. Lumin.* **3132, Part 2,** 783–785 (1984).
26. Sundström, V., Gillbro, T., Gadonas, R. A. & Piskarskas, A. Annihilation of singlet excitons in j aggregates of pseudoisocyanine (pic) studied by pico- and subpicosecond spectroscopy. *J. Chem. Phys.* **89,** 2754–2762 (1988).
27. Stiel, H., Daehne, S. & Teuchner, K. J-aggregates of pseudoisocyanine in solution: New data from nonlinear spectroscopy. *J. Lumin.* **39,** 351–357 (1988).
28. Moll, J., Harrison, W. J., Brumbaugh, D. V. & Muenter, A. A. Exciton annihilation in j-aggregates probed by femtosecond fluorescence upconversion. *J. Phys. Chem. A* **104,** 8847–8854 (2000).
29. Akselrod, G. M., Tischler, Y. R., Young, E. R., Nocera, D. G. & Bulović, V. Exciton–exciton annihilation in organic polariton microcavities. *Phys. Rev. B* **82,** 113106 (2010).
30. Andreani, L., Savona, V., Schwendimann, P. & Quattropani, A. Polaritons in high reflectivity microcavities: semiclassical and full quantum treatment of optical properties. *Superlatt. Microstruct.* **15,** 453–458 (1994).
31. Skolnick, M. S., Fisher, T. A. & Whittaker, D. M. Strong coupling phenomena in quantum microcavity structures. *Semicond. Sci. Technol.* **13,** 645–669 (1998).
32. Agranovich, V. M., Litinskaia, M. & Lidzey, D. G. Cavity polaritons in microcavities containing disordered organic semiconductors. *Phys. Rev. B* **67,** 085311 (2003).
33. Coles, D. M., Grant, R. T., Lidzey, D. G., Clark, C. & Lagoudakis, P. G. Imaging the polariton relaxation bottleneck in strongly coupled organic semiconductor microcavities. *Phys. Rev. B* **88,** 121303 (2013).
34. Michetti, P. & La Rocca, G. C. Simulation of j-aggregate microcavity photoluminescence. *Phys. Rev. B* **77,** 195301 (2008).
35. Michetti, P. & La Rocca, G. C. Exciton–phonon scattering and photoexcitation dynamics in *j*-aggregate microcavities. *Phys. Rev. B* **79,** 035325 (2009).
36. Michetti, P. & La Rocca, G. C. Simulation of the time dependent photoluminescence of a j-aggregate microcavity. *Phys. Status Solidi C* **6,** 403–406 (2009).
37. Agranovich, V. M., Litinskaya, M. & Lidzey, D. G. Microcavity polaritons in materials with weak intermolecular interaction. *Phys. Status Solidi B* **234,** 130–138 (2002).
38. Litinskaya, M., Reineker, P. & Agranovich, V. M. Fast polariton relaxation in strongly coupled organic microcavities. *J. Lumin.* **110,** 364–372 (2004).
39. Litinskaya, M., Reineker, P. & Agranovich, V. M. Exciton–polaritons in organic microcavities. *J. Lumin.* **119–120,** 277–282 (2006).
40. Chovan, J., Perakis, I. E., Ceccarelli, S. & Lidzey, D. G. Controlling the interactions between polaritons and molecular vibrations in strongly coupled organic semiconductor microcavities. *Phys. Rev. B* **78,** 045320 (2008).
41. Michetti, P. & La Rocca, G. C. Polariton states in disordered organic microcavities. *Phys. Rev. B* **71,** 115320 (2005).
42. Michetti, P. & Rocca, G. L. Polariton dynamics in disordered microcavities. *Physica E* **40,** 1926–1929 (2008).
43. Lidzey, D. G. *et al.* Experimental study of light emission from strongly coupled organic semiconductor microcavities following nonresonant laser excitation. *Phys. Rev. B* **65,** 195312 (2002).
44. Coles, D. M., Michetti, P., Clark, C., Adawi, A. M. & Lidzey, D. G. Temperature dependence of the upper-branch polariton population in an organic semiconductor microcavity. *Phys. Rev. B* **84,** 205214 (2011).
45. Coles, D. M. *et al.* Vibrationally assisted polariton-relaxation processes in strongly coupled organic-semiconductor microcavities. *Adv. Funct. Mater.* **21,** 3691–3696 (2011).
46. Müller, M., Bleuse, J., André, A. & Ulmer-Tuffigo, H. Observation of bottleneck effects on the photoluminescence from polaritons in ii–iv microcavities. *Physica B* **272,** 476–479 (1999).
47. Tartakovskii, A. I. *et al.* Relaxation bottleneck and its suppression in semiconductor microcavities. *Phys. Rev. B* **62,** R2283–R2286 (2000).

48. Virgili, T. *et al.* Ultrafast polariton relaxation dynamics in an organic semiconductor microcavity. *Phys. Rev. B* **83,** 245309 (2011).

Acknowledgements
We gratefully acknowledge R.T. Grant for the atomic force micrographs presented in the Supplementary Information. We acknowledge financial support for the work via the UK EPSRC through grant EP/G062404/1 and by the European Union through the FP7 funded project Icarus (237900).

Author contributions
D.G.L. and D.M.C. conceived the experiment. Samples were prepared by C.C. and D.M.C. Steady-state measurements were performed by D.M.C. N.S. performed time-resolved measurements under the supervision of P.G.L. and P.G.S. The model was developed by P.M. All authors contributed to the interpretation of results and preparation of the manuscript.

Additional information
Supplementary information is available in the online version of the paper. Reprints and permissions information is available online at www.nature.com/reprints. Correspondence and requests for materials should be addressed to D.G.L.

Competing financial interests
The authors declare no competing financial interests.